J Therm Anal Calorim (2012) 110:781–787
DOI 10.1007/s10973-011-1968-9

Products and non-isothermal kinetics of thermal decomposition of $MgFe_2(C_2O_4)_3{\cdot}6H_2O$

Xuehang Wu · Wenwei Wu · Kaiwen Zhou · Xuemin Cui · Sen Liao

Received: 3 September 2011 / Accepted: 29 September 2011 / Published online: 27 October 2011

Abstract $MgFe_2(C_2O_4)_3{\cdot}6H_2O$ was synthesized by solid-state reaction at low heat using $MgSO_4{\cdot}7H_2O$, $FeSO_4{\cdot}7H_2O$, and $Na_2C_2O_4$ as raw materials. The spinel $MgFe_2O_4$ was obtained via calcining $MgFe_2(C_2O_4)_3{\cdot}6H_2O$ above 500 °C in air. The $MgFe_2(C_2O_4)_3{\cdot}6H_2O$ and its calcined products were characterized by thermogravimetry and differential scanning calorimetry (TG/DSC), Fourier transform FT-IR, X-ray powder diffraction (XRD), and vibrating sample magnetometer (VSM). The result showed that $MgFe_2O_4$ obtained at 800 °C had a specific saturation magnetization of 40.4 emu g^{-1}. The thermal process of $MgFe_2(C_2O_4)_3{\cdot}6H_2O$ experienced three steps, which involves the dehydration of the six waters of crystallization at first, and then decomposition of $MgFe_2(C_2O_4)_3$ into amorphous $MgFe_2O_4$ in air, and at last crystallization of $MgFe_2O_4$. Based on Flynn–Wall–Ozawa equation, the average values of the activation energies associated with the thermal decomposition of $MgFe_2(C_2O_4)_3{\cdot}6H_2O$ were determined to be 148.45 ± 25.50 and 184.08 ± 7.64 kJ mol^{-1} for the first and second decomposition steps, respectively. Dehydration of the six waters of $MgFe_2(C_2O_4)_3{\cdot}6H_2O$ is multi-step reaction mechanisms. Decomposition of $MgFe_2(C_2O_4)_3$ into $MgFe_2O_4$ could be simple reaction mechanisms, kinetic model that can better describe the thermal decomposition of $MgFe_2(C_2O_4)_3$ is the $F_{3/4}$ model, and the corresponding function is $g(\alpha) = 1 - (1 - \alpha)^{1/4}$.

X. Wu · W. Wu (✉) · K. Zhou · X. Cui · S. Liao
School of Chemistry and Chemical Engineering, Guangxi University, Nanning 530004, China
e-mail: gxuwuwenwei@yahoo.com.cn

K. Zhou
School of Materials Science and Engineering, Guangxi University, Nanning 530004, China

Keywords Inorganic compounds · Chemical synthesis · Non-isothermal kinetics · Thermal decomposition

Introduction

There has been an increasing interest in magnetic ferrites nanoparticles because of their broad application in many fields including ferrofluids [1], magnetic drug delivery [2], hyperthermia treatment [3], magnetic high-density information storage [4], catalysis [5], energy storage [6], and gas sensors [7]. Ferrites can occur in several different crystal structure forms. Within this group, spinel is a kind of the most important structure that occurs in three forms: normal, inverse, and randomic spinel structure. Spinel magnesium ferrites are a soft magnetic *n*-type semiconducting material [8]. The structural formula of magnesium ferrites is generally written as $(Mg_{1-\lambda}Fe_{\lambda})[Mg_{\lambda}Fe_{2-\lambda}]O_4$, where parentheses and square brackets indicate cation site of tetrahedral (A) and octahedral (B) coordination, respectively, and where λ represents the degree of inversion defined as a fraction of (A) sites occupied by Fe^{3+} ions.

To date, various methods have been developed to synthesize $MgFe_2O_4$, including ceramic method [6], mechanochemical [9, 10], coprecipitation [11, 12], sol–gel method [13, 14], reverse micelle method [15], hydrothermal reaction [3, 16], etc. It was found that $MgFe_2O_4$ crystallite diameter associated with performance was highly dependent on the synthesis and processing methods, such as, Sivakumar et al. [10] synthesized spinel $MgFe_2O_4$ with various grain sizes ranging from 19 to 72 nm using ceramic method and followed by mechanochemical method. Hankare et al. [12] synthesized $MgFe_2O_4$ with grain size of 40 nm by coprecipitation method. Chandradass et al. [15] obtained $MgFe_2O_4$ nanocrystals by reverse micelle method, and the

results showed that the average particle size, morphology, and saturation magnetization of $MgFe_2O_4$ nanocrystals were dependent on the continuous phase, the values of specific saturation magnetization for heptane, toluene, and cyclohexane as continuous phase are 14.5, 30, and 37 emu g^{-1}, respectively. Verma et al. [16] produced $MgFe_2O_4$ nanoparticles with about 3 nm by microwave hydrothermal method, which exhibits superparamagnetic behavior.

The aim of this study is to prepare pure phase nanocrystalline $MgFe_2O_4$ via solid-state reaction at low heat [17] and to study magnetic properties of $MgFe_2O_4$ and the kinetics of the thermal decomposition of precursor. The kinetics of the thermal decomposition of precursor was studied using TG-DSC technique. Non-isothermal kinetics of the thermal decomposition of precursor was interpreted by Flynm–Wall–Ozawa (FWO) method [18, 19]. The kinetic (E_a, ln A, mechanism) parameters of the thermal decomposition of precursor $MgFe_2(C_2O_4)_3{\cdot}6H_2O$ are discussed for the first time.

Experimental

Reagent and apparatus

All chemicals were of reagent grade purity. TG/DSC measurements were made using a Netsch 40PC thermogravimetric analyzer. X-ray powder diffraction (XRD) was performed using a Rigaku D/max 2500 V diffractometer equipped with a graphite monochromator and a Cu target. The FT-IR spectra of the precursor and its calcined products were recorded on a Nexus 470 FT-IR instrument. The morphologies of the calcined samples and energy dispersive X-ray spectrometer (EDS) were obtained on S-3400 scanning electron microscopy (SEM). The specific saturation magnetizations (Ms) of the calcined sample powders were carried out at room temperature using a magnetic property measurement system (SQUID-MPMS-XL-5).

Preparation of $MgFe_2(C_2O_4)_3{\cdot}6H_2O$

The $MgFe_2(C_2O_4)_3{\cdot}6H_2O$ were prepared by solid-state reaction at low heat [17] using $MgSO_4{\cdot}7H_2O$, $FeSO_4{\cdot}7H_2O$, and $Na_2C_2O_4$ as starting materials. In a typical synthesis, $MgSO_4{\cdot}7H_2O$ (24.25 g), $FeSO_4{\cdot}7H_2O$ (54.71 g), and $Na_2C_2O_4$ (45.49 g), and surfactant polyethylene glycol (PEG)-400 (3.0 mL, 50 vol.%) were put in a mortar, and the mixture was fully ground by hand with a rubbing mallet for 40 min. The grinding velocity was about 200 circles/min, and the strength applied was moderate. The reactant mixture gradually became damp, and then a paste formed quickly. The reaction mixture was kept at room temperature for 2 h. The solid was washed with deionized water to remove soluble inorganic salts until SO_4^{2-} ion could not be visually detected with a 0.5 mol L^{-1} $BaCl_2$ solution. The solid was then washed with a small amount of anhydrous ethanol and dried at 80 °C for 3 h. The resulting material was subsequently determined to be the $MgFe_2(C_2O_4)_3{\cdot}6H_2O$. Nanocrystalline $MgFe_2O_4$ was obtained via calcining $MgFe_2(C_2O_4)_3{\cdot}6H_2O$ above 500 °C in air.

Determination of activation energy by FWO method [18, 19]

Kinetic equation of solid-state reaction can be expressed as Eq. 1:

$$\frac{d\alpha}{dt} = Ae^{-E_a/RT}f(\alpha) \tag{1}$$

When heating rate is kept at fixed value, that is: $\beta = dT/dt$. Equation 1 can be rewritten into Eq. 2:

$$\frac{d\alpha}{dT} = \frac{A}{\beta}e^{-E_a/RT}f(\alpha) \tag{2}$$

where E_a is apparent activation energy, A is pre-exponential factor, R is the gas constant, and α is called reaction degree. The $f(\alpha)$ is a function of α, which reveals the mechanism of reaction. By a series of transforms, thus Eq. 2 can be rewritten as the Eq. 3:

$$\log\beta = [\log\frac{AE_a}{R} - \log g(\alpha) - 2.315] - 0.4567\frac{E_a}{RT} \tag{3}$$

If α is a fixed value, thus log $g(\alpha)$ is a fixed value, too. The dependence of log β on $1/T$ must give rise to a straight line. Thus, reaction activation energy E_a can be obtained from linear slope ($-0.4567E_a/R$). According to Eq. 3, a plot of log $g(\alpha)$ versus $1/T$ is plotted when heating rate β is kept fixed value. The $g(\alpha)$ corresponding to straight line with high correlation coefficient is selected to represent mechanism function of thermal decomposition process.

Results and discussion

TG/DSC analysis of $MgFe_2(C_2O_4)_3{\cdot}6H_2O$

Figure 1 shows the TG/DSC curves of the synthetic product at four different heating rates in air, respectively.

The TG/DSC curves show that thermal decomposition of the $MgFe_2(C_2O_4)_3{\cdot}6H_2O$ below 600 °C occurs in two well-defined steps. The first step starts at about 80 °C, ends at about 209 °C, and characterized by a strong endothermic DSC peak at 228 °C that can be attributed to the six water molecules eliminated from $MgFe_2(C_2O_4)_3{\cdot}6H_2O$ and the formation of $MgFe_2(C_2O_4)_3$. The observed mass loss in the TG curve is 21.12%, which is in good agreement with

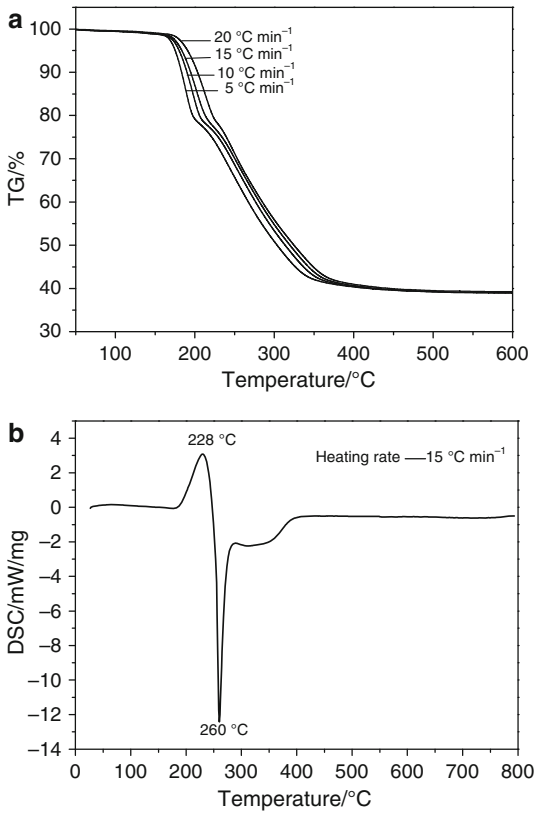

Fig. 1 TG/DSC curves of the $MgFe_2(C_2O_4)_3{\cdot}6H_2O$ at different heating rates in air

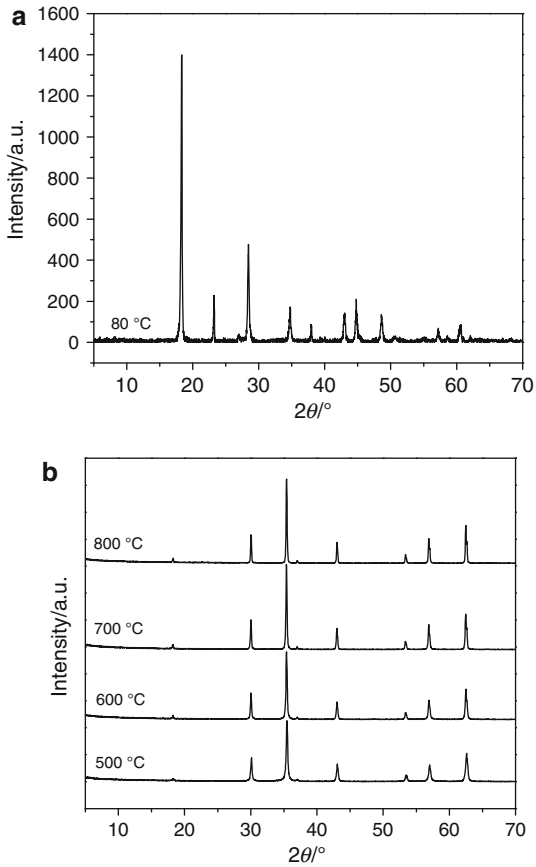

Fig. 2 XRD patterns of $MgFe_2(C_2O_4)_3{\cdot}6H_2O$ and its calcined samples at different temperatures for 1 h

21.27% theoretic mass loss of six water molecules eliminated from $MgFe_2(C_2O_4)_3{\cdot}6H_2O$. The second decomposition step begins at about 209 °C, and ends at 500 °C, which involves an exothermic process with a strong DSC peak at 260 °C, attributed to the decomposition of $MgFe_2(C_2O_4)_3$ and the formation of $MgFe_2O_4$. The corresponding observed mass loss in the TG curve is 39.35%, which is in good agreement with 39.37% theoretic mass loss of reaction of $MgFe_2(C_2O_4)_3$ with two O_2 molecules and formation of $MgFe_2O_4$. The broad exothermic DSC peak at about 350 °C can be attributed to crystallization of cubic phase $MgFe_2O_4$.

XRD analysis of $MgFe_2(C_2O_4)_3{\cdot}6H_2O$ and its calcined samples

Figure 2 shows the XRD patterns of $MgFe_2(C_2O_4)_3{\cdot}6H_2O$ dried at 80 °C and the products resulting from calcination at different temperatures for 1 h.

From Fig. 2a, the results show that strong intensity and smoothed baseline, a wide and low diffraction pattern of the product is observed. This indicates that the $MgFe_2(C_2O_4)_3{\cdot}6H_2O$ obtained at 80 °C is crystalline with a higher crystallinity. From Fig. 2b, when the sample was heated at 500 °C for 1 h, all the diffraction peaks in the pattern are in agreement with that of cubic $MgFe_2O_4$, with space group Fd-3m(227), lattice parameters: $a = b = c = 0.84$ nm, $\alpha = \beta = \gamma = 90°$, density = 4.482 g cm^{-3}, from PDF card 88-1942. Intensity of diffraction peaks of cubic $MgFe_2O_4$ increases with increasing calcination temperature, which indicates that degree of crystallization of cubic $MgFe_2O_4$ increases with increasing calcination temperature.

According to the Scherrer formula [20]: $D = K\lambda/(\beta\cos\theta)$, where D is crystallite diameter, $K = 0.89$ (the Scherrer constant), $\lambda = 0.15406$ nm (wavelength of the X-ray used), β is the width of line at the half-maximum intensity, and θ is the corresponding angle. The resulting crystallite sizes of the products from calcining precursor at the temperatures of 500, 600, 700, and 800 °C for 1 h, are 32, 41, 46, and 54 nm, respectively.

IR spectroscopic analysis of $MgFe_2(C_2O_4)_3{\cdot}6H_2O$ and its calcined samples

The FT-IR spectra of $MgFe_2(C_2O_4)_3{\cdot}6H_2O$ and its calcined sample are shown in Fig. 3. The $MgFe_2(C_2O_4)_3{\cdot}6H_2O$

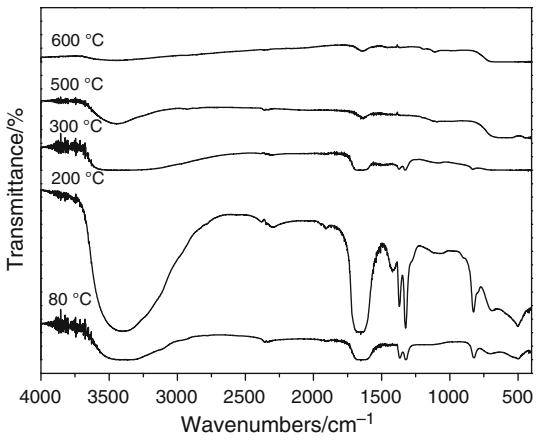

Fig. 3 FT-IR spectra of $MgFe_2(C_2O_4)_3{\cdot}6H_2O$ and its calcined samples

exhibits a strong and broad band at about 3425 cm^{-1} that can be assigned to symmetric and asymmetric stretching modes of water molecules. The bending mode of water expected around 1643 cm^{-1} is overlapped with the intense oxalate band which is around 1620 cm^{-1} [21–23]. The bands at 1325 and 1371 cm^{-1} can be assigned to either the appearance of new M–OC_2O_3 (M = Mg, Fe) bonds and/or to the combinations of OH librations and lattice modes [24, 25]. The bands at about 3425 and 1643 cm^{-1} were assigned to absorption water from air when sample was calcined at 500 °C.

SEM and EDS analysis of the calcined sample

The morphologies and EDS spectrum of the calcined samples are shown in Fig. 4. From Fig. 4a, it can be seen that the calcined sample at 600 °C is composed of polyhedral grains, which contains particles having a distribution of small particles (50–100 nm) and large particles (100–250 nm). With the increase of calcining temperature, the calcined sample is aggregated into larger polyhedral grains further. Figure 4c shows the SEM micrographs of sample obtained at 800 °C. It can be seen that the particle sizes of calcined sample obtained at 800 °C are about 400 nm. The average crystallite sizes of the calcined samples determined by X-ray diffraction are significantly smaller than the values determined by SEM. This is attributed that values observed by SEM technique give the size of the secondary particles, and the X-ray line broadening analysis discloses only the size of primary particles. EDS spectrum of the calcined product at 700 °C shows that mole ratio of Mg:Fe is equal to 0.99:2.0, which is in agreement with that obtained by XRD analysis. Therefore, composition of the calcined product is determined to be $MgFe_2O_4$.

Magnetic properties of the calcined samples

The hysteresis loop of $MgFe_2O_4$ samples calcined at different temperatures is shown in Fig. 5. It can be observed that specific saturation magnetizations of powders calcined at 600, 700, and 800 °C for 1 h are 30.4, 35.7, and 40.4 emu g^{-1}, respectively. That is: specific saturation magnetization of $MgFe_2O_4$ increases with increasing calcination temperature. In other words, the larger the crystallite size of the particles, the larger is the specific saturation magnetizations. For the sample calcined at 600 °C with crystallite size of 41 nm, the Ms value is 30.4 emu g^{-1}. When the calcination temperature is 800 °C, the crystallite size of sample is 54 nm, and the Ms value is 40.4 emu g^{-1}. The lower Ms values associated with smaller crystallite sizes can be attributed to two reasons. First, surface distortions due to the interaction of the transition metal Fe^{3+} ions with the oxygen atoms in the spinel lattice of $MgFe_2O_4$ can reduce the net magnetic moment in the particle. Second, the magnetocrystalline anisotropy of the particles is dependent on the crystallinity of $MgFe_2O_4$. The higher calcination temperature, the larger crystallinity of $MgFe_2O_4$. As can be observed in the XRD pattern mentioned above, samples calcined at lower temperatures have lower crystallinity. Hence, a large proportion of crystal defects and dislocations can occur within the lattice, which causes magnetocrystalline anisotropy distortion and a reduction of magnetic moment within the particles of $MgFe_2O_4$ [26]. Compared with magnetic properties of $MgFe_2O_4$ obtained by other method [10, 14], $MgFe_2O_4$ synthesized by solid-state reaction at low heat exhibits higher specific saturation magnetizations, which can be attributed that $MgFe_2O_4$ obtained by the latter method has higher crystallinity and more perfect crystalline morphology than that obtained by the former methods.

Kinetics of thermal decomposition of $MgFe_2(C_2O_4)_3{\cdot}6H_2O$

In accordance with TG/DSC analysis and XRD analysis of $MgFe_2(C_2O_4)_3{\cdot}6H_2O$ and its calcined products mentioned above, thermal process of $MgFe_2(C_2O_4)_3{\cdot}6H_2O$ below 800 °C consists of three steps, which can be expressed as follows, respectively.

$$MgFe_2(C_2O_4)_3{\cdot}6H_2O\ (cr) \longrightarrow MgFe_2(C_2O_4)_3(s) + 6H_2O(g) \quad (4)$$

$$MgFe_2(C_2O_4)_3(s) + 2O_2(g) \longrightarrow MgFe_2O_4(am) + 6CO_2(g) \quad (5)$$

$$MgFe_2O_4(am) \longrightarrow MgFe_2O_4(c) \quad (6)$$

According to non-isothermal method, the basic data of α and T collected from the TG curves of the thermal decomposition of $MgFe_2(C_2O_4)_3{\cdot}6H_2O$ at various heating

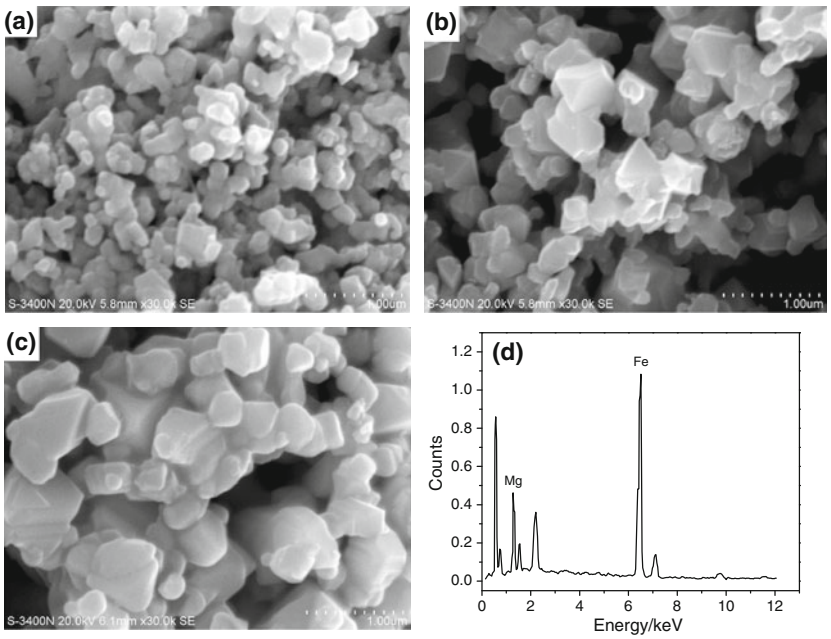

Fig. 4 SEM and EDS analysis of the calcined sample: **a** 600 °C, **b** 700 °C, and **c** 800 °C

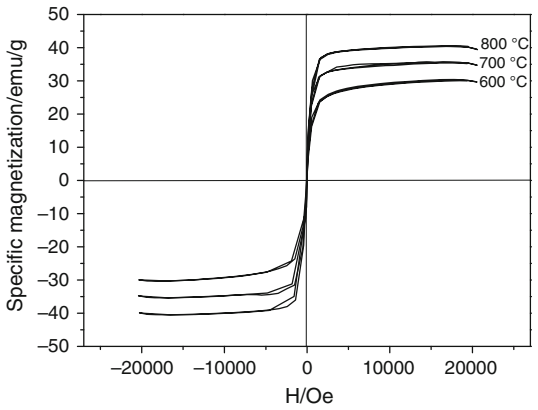

Fig. 5 Hysteresis loops for $MgFe_2O_4$ samples obtained at different temperatures for 1 h

rates (5, 10, 15, and 20 K min^{-1}) are illustrated in Tables 1 and 2. According to Eq. 3, the plots of log β versus 1000/T corresponding to different conversions α can be obtained by a linear regression of least-square method, respectively. The FWO analysis results of four TG measurements below 500 °C (773 K) are shown in Fig. 6. In accordance with FWO equation, the slopes of these straight lines can be determined, then average activation energy for the thermal decomposition reaction of $MgFe_2(C_2O_4)_3{\cdot}6H_2O$ was obtained. Table 3 shows the activation energy and correlation coefficient (r^2) calculated by FWO method for the thermal decomposition steps of $MgFe_2(C_2O_4)_3{\cdot}6H_2O$.

From Table 3, the activation energies change of the step 1 with α is higher than 10%, and that of the step 2 with α are lower than 10%, so that we draw a conclusion that the dehydration of six crystal water of $MgFe_2(C_2O_4)_3{\cdot}6H_2O$ could be multi-step reaction mechanisms [27–30], and

Table 1 Correlative data used for drawing plot of log β versus 1000/T for step 1

α	β/K min^{-1}			
	5 (T/K)	10 (T/K)	15 (T/K)	20 (T/K)
0.2	448.30	454.30	457.75	462.05
0.3	451.95	457.80	462.75	466.75
0.4	455.00	461.55	465.95	470.50
0.5	457.75	464.85	469.70	474.65
0.6	460.35	467.95	473.15	477.50
0.7	462.85	470.90	476.55	482.10
0.8	465.45	473.90	480.05	485.75

Table 2 Correlative data used for drawing plot of log β versus 1000/T for step 2

α	β/K min^{-1}			
	5 (T/K)	10 (T/K)	15 (T/K)	20 (T/K)
0.2	507.85	516.30	520.70	524.00
0.3	519.40	527.95	532.30	535.15
0.4	531.00	539.85	544.50	547.70
0.5	543.05	552.30	557.30	561.05
0.6	556.30	565.90	571.35	575.70
0.7	571.30	581.30	587.30	592.20
0.8	588.05	598.35	604.55	610.05

decomposition of $MgFe_2(C_2O_4)_3$ into $MgFe_2O_4$ could be simple reaction mechanisms. According to Eq. 3, mechanism function $g(\alpha)$ and pre-exponential factor log A can be obtained. The results show that the kinetic model, which can better describe the thermal decomposition of

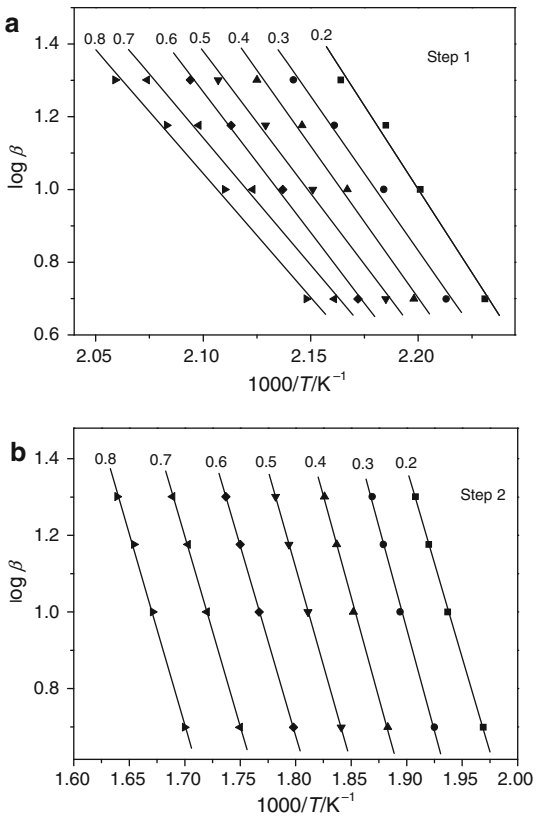

Fig. 6 FWO analysis for the thermal decomposition of $MgFe_2(C_2O_4)_3{\cdot}6H_2O$

Table 3 Activation energies (E_a) and correlation coefficient (r^2) calculated by FWO method

α	Step 1		Step 2	
	E_a/kJ mol^{-1}	r^2	E_a/kJ mol^{-1}	r^2
0.2	168.37	0.9882	180.51	0.9989
0.3	155.80	0.9881	191.72	0.9968
0.4	153.23	0.9903	189.91	0.9983
0.5	142.52	0.9903	185.59	0.9994
0.6	141.27	0.9966	181.72	0.9998
0.7	128.29	0.9909	178.74	0.9993
0.8	122.95	0.9916	180.38	0.9984
Average	148.45 ± 25.50	0.9909	184.08 ± 7.64	0.9987

$MgFe_2(C_2O_4)_3$, is the $F_{3/4}$ model, the corresponding function is $g(\alpha) = 1 - (1 - \alpha)^{1/4}$, and pre-exponential factor log A is equal to 16.20.

Conclusions

This research has successfully synthesized $MgFe_2(C_2O_4)_3{\cdot}6H_2O$ and cubic phase $MgFe_2O_4$. XRD analysis suggests that cubic $MgFe_2O_4$ can be obtained via calcining $MgFe_2(C_2O_4)_3{\cdot}6H_2O$ above 500 °C in air. Magnetic characterization of $MgFe_2O_4$ indicates that the calcined temperature has a marked effect on specific saturation magnetization of powder caused an increase of specific saturation magnetization from 30.4 to 40.4 emu g^{-1} with an increase of calcined temperature from 600 to 800 °C. The thermal process of $MgFe_2(C_2O_4)_3{\cdot}6H_2O$ in the range of ambient temperature to 800 °C experiences three steps, which involves the dehydration of the six crystal water molecules at first, and then decomposition of $MgFe_2(C_2O_4)_3$ into $MgFe_2O_4$ in air, and at last crystallization of $MgFe_2O_4$. The kinetics of the thermal decomposition of $MgFe_2(C_2O_4)_3{\cdot}6H_2O$ was studied using non-isothermal TG technique. The average values of the activation energies associated with the thermal process of $MgFe_2(C_2O_4)_3{\cdot}6H_2O$ are 148.45 ± 25.50 and 184.08±7.64 kJ mol^{-1} for the first and second decomposition steps, respectively. Dehydration of the six waters of crystallization of $MgFe_2(C_2O_4)_3{\cdot}6H_2O$ is multi-step reaction mechanisms, and decomposition of $MgFe_2(C_2O_4)_3$ into $MgFe_2O_4$ could be simple reaction mechanisms.

Acknowledgements This study was financially supported by the National Nature Science Foundation of China (Grant no. 21161002) and the Guangxi Nature Science Foundation of China (Grant no. 2011GXNSFA018036).

References

1. Pileni MP. Magnetic fluids: fabrication, magnetic properties, and organization of nanocrystals. Adv Funct Mater. 2001;5:323–36.
2. Pankhurst QA, Connolly J, Jones SK, Dobson J. Applications of magnetic nanoparticles in biomedicine. J Phys D Appl Phys. 2003;36:167.
3. Sasaki T, Ohara S, Naka T, Vejpravova J, Sechovsky V, Umetsu M, Takami S, Jeyadevan B, Adschiri T. Continuous synthesis of fine $MgFe_2O_4$ nanoparticles by supercritical hydrothermal reaction. J Supercrit Fluids. 2010;53:92–4.
4. Song Q, Zhang ZJ. Shape control and associated magnetic properties of spinel cobalt ferrite nanocrystals. J Am Chem Soc. 2004;126:6164–8.
5. Pankhurst QA, Pollard RJ. Fine-particle magnetic oxides. J Phys Condens Matter. 1993;5:8487–508.
6. Sivakumar N, Gnanakan SRP, Karthikeyan K, Amaresh S, Yoon WS, Park GJ, Lee YS. Nanostructured $MgFe_2O_4$ as anode materials for lithium-ion batteries. J Alloys Compd. 2011;509:7038–41.
7. Rezlescu N, Iftimie N, Rezlescu E, Doroftei C, Popa PD. Semiconducting gas sensor for acetone based on the fine grained nickel ferrite. Sens Actuators B. 2006;114:427–32.
8. Willey RJ, Noirclerc P, Busca G. Preparation and characterization of magnesium chromite and magnesium ferrite aerogels. Chem Eng Commun. 1993;123:1–16.
9. Bergmann I, Šepelák V, Becker KD. Preparation of nanoscale $MgFe_2O_4$ via non-conventional mechanochemical. Solid State Ionics. 2006;177:1865–8.
10. Sivakumara N, Narayanasamy A, Greneche JM, Murugaraj R, Leed YS. Electrical and magnetic behaviour of nanostructured $MgFe_2O_4$ spinel ferrite. J Alloys Compd. 2010;504:395–402.

11. Chen Q, Rondinone AJ, Chakoumakos BC, Zhang ZJ. Synthesis of superparamagnetic $MgFe_2O_4$ nanoparticles by coprecipitation. J Magn Magn Mater. 1999;194:1–7.
12. Hankare PP, Jadhav SD, Sankpal UB, Patil RP, Sasikala R, Mulla IS. Gas sensing properties of magnesium ferrite prepared by co-precipitation method. J Alloys Compd. 2009;488:270–2.
13. Pradeep A, Priyadharsini P, Chandrasekaran G. Sol–gel route of synthesis of nanoparticles of $MgFe_2O_4$ and XRD, FTIR and VSM study. J Magn Magn Mater. 2008;320:2774–9.
14. Huang YJ, Tang Y, Wang J, Chen QW. Synthesis of $MgFe_2O_4$ nanocrystallites under mild conditions. Mater Chem Phys. 2006; 97:394–7.
15. Chandradass J, Kim KH. Solvent effects in the synthesis of $MgFe_2O_4$ nanopowders by reverse micelle processing. J Alloys Compd. 2011;509:59–62.
16. Verma S, Joy PA, Khollam YB, Potdar HS, Deshpande SB. Synthesis of nanosized $MgFe_2O_4$ powders by microwave hydrothermal method. Mater Lett. 2004;58:1092–5.
17. Wu WW, Li SS, Liao S, Xiang F, Wu XH. Preparation of new sunscreen materials $Ce_{1-x}Zn_xO_{2-x}$ via solid-state reaction at room temperature and study on their properties. Rare Metals. 2010;29:149–53.
18. Flynn JH, Wall LA. A quick direct method for the determination of activation energy from thermogravimetric data. Polym Lett. 1966;4:323–8.
19. Ozawa TA. New method of analyzing thermogravimetric data. Bull Chem Soc Jpn. 1965;38:1881–6.
20. Wu XH, Wu WW, Cui XM, Liao S. Preparation of nanocrystalline $BiFeO_3$ via a simple and novel method and its kinetics of crystallization, J Therm Anal Calorim. 2011. doi:10.1007/s10973-011-1483-z.
21. Wu XH, Wu WW, Liu C, Li SS, Liao S, Cai JC. Synthesis of layered sodium manganese phosphate via low-heating solid-state reaction and its properties. Chin J Chem. 2010;28:2394–8.
22. Wu XH, Wu WW, Cui XM, Liao S. Selective self-assembly synthesis of $MnV_2O_6{\cdot}4H_2O$ with controlled morphologies and study on its thermal decomposition. J Therm Anal Calorim. 2011. doi:10.1007/s10973-011-1577-7.
23. Elizabeth A, Joseph C, Paul I, Ittyachen MA, Mathew KT, Lonappan A, Jacob J. Microwave studies on double rare earth oxalate crystals. Mater Sci Eng A. 2005;391:43–50.
24. Donia AM. Synthesis, identification and thermal analysis of co-precipitates of silver-(cobalt, nickel, copper and zinc) oxalate. Polyhedron. 1997;16:3013–31.
25. Goel SP, Mehrotra PN. IR and thermal studies on lithium oxomolybdenum (VI) oxalate. J Thermal Anal. 1985;30:145–51.
26. Jiang CT, Liu RJ, Shen XQ, Zhu L, Song FZ. $Ni_{0.5}Zn_{0.5}Fe_2O_4$ nanoparticles and their magnetic properties and adsorption of bovine serum albumin. Powder Technol. 2011;211:90–4.
27. Vlaev L, Nedelchev N, Gyurova K, Zagorcheva M. A comparative study of \-isothermal kinetics of decomposition of calcium oxalate monohydrate. J Anal Appl Pyrolysis. 2008;81:253–62.
28. Genieva SD, Vlaev LT, Atanassov AN. Study of the thermo-oxidative degradation kinetics of poly(tetrafluoroethene) using iso-conversional calculation procedure. J Therm Anal Calorim. 2010;99:551–61.
29. Wu XH, Wu WW, Li SS, Cui XM, Liao S. Kinetics and thermodynamics of thermal decomposition of $NH_4NiPO_4{\cdot}6H_2O$. J Therm Anal Calorim. 2011;103:805–12.
30. Boonchom B, Danvirutai C. Kinetics and thermodynamics of thermal decomposition of synthetic $AlPO_4{\cdot}2H_2O$. J Therm Anal Calorim. 2009;98:771–7.